IMAGING METHODOLOGY - Full Papers

Magnetic Resonance in Medicine 75:519–526 (2016)

Detection of Subnanotesla Oscillatory Magnetic Fields Using MRI

Xia Jiang,[1] Jingwei Sheng,[2,3] Huanjie Li,[2,3] Yuhui Chai,[2,3] Xin Zhou,[4] Bing Wu,[5] Xiaodong Guo,[1] and Jia-Hong Gao[2,3,6]*

Purpose: Direct mapping of neuronal currents using MRI would have fundamental impacts on brain functional imaging. Previous reports indicated that the stimulus-induced rotary saturation (SIRS) mechanism had the best potential of direct detection of neural oscillations; however, it lacked the high-sensitivity level needed. In this study, a novel strategy is proposed in an effort to improve the detection sensitivity.

Methods: In our modified SIRS sequence, an external oscillatory magnetic field is used as the excitation pulse in place of the standard 90-degree excitation pulse. This approach could potentially lead to tens or even hundreds times of enhancement in the detection sensitivity for low field signals. It also helps to lower the physiological noise, allows for shorter pulse repetition time, and is less affected by the blood oxygen level.

Results: We demonstrate that a 100-Hz oscillatory magnetic field with magnitude as low as 0.25 nanotesla generated in a current loop can be robustly detected using a 3-Tesla MRI scanner.

Conclusion: The modified SIRS sequence offers higher detection sensitivity as well as several additional advantages. These promising results suggest that the direct detection of neural oscillation might be within the grasp of the current MRI technology. **Magn Reson Med 75:519–526, 2016. © 2015 Wiley Periodicals, Inc.**

Key words: functional magnetic resonance imaging; neuronal current; neural oscillation; stimulus induced rotary saturation; doubly rotating frame

INTRODUCTION

Functional magnetic resonance imaging (fMRI) is one of the leading research tools for noninvasive imaging of brain activity. Conventional fMRI, based on the blood oxygen level-dependent (BOLD) mechanism, only detects neural activation indirectly through neurovascular coupling; consequently, it is limited in its spatial and temporal resolutions. To overcome this limitation, efforts have been devoted to develop alternative fMRI mechanisms that are independent of cerebral hemodynamics (1). One promising approach is the neuronal current MRI (ncMRI) (2), in which the small neuronal magnetic field (NMF) produced by the electrical currents generated during neural activations is detected by an MRI scanner. Whereas phantom studies yielded encouraging results (3–5), in vivo studies only produced inconclusive and mixed results (6–15), leaving the feasibility of in vivo ncMRI an issue for debate.

Most previous in vivo ncMRI studies that were aimed at detecting evoked potentials were based on a phase-shift approach in which a direct current distribution (and the consequent NMF) is induced by sensory stimulation, and the MRI acquisition window is carefully aligned with the duration of the current such that a phase shift is produced in the precession of the nuclear spin. Depending on the geometry and alignment of the local neurons, the net effect of the NMF on the MR signal at the voxel level can be either a phase shift, a reduction in the magnitude, or both (16). Whereas the evoked potentials can be easily predicted and their timing can be controlled, their magnitude is very low. The NMF caused by evoked potentials has been estimated to be 0.1 to 1 nanotesla (nT) (3), mainly due to postsynaptic activity, making its detection with ncMRI an extremely challenging task (8,11,12,17).

A more likely target for ncMRI detection might be the spontaneous neural oscillation, which is known to produce larger NMF than that from an evoked potential. For example, the strongest type of neural oscillation, the alpha activity, produces an equivalent current dipole of $\sim$100 nano ampere meters (nAm), whereas typically evoked potentials produce current dipoles of $\sim$10 nAm (18). In addition, neural oscillations in different frequency bands are known to be associated with a number of important perceptual and cognitive functions (19–24). Thus, being able to detect such activates with ncMRI would provide great utility. The phase-shift ncMRI technique can only be used to detect an oscillatory field within or below the alpha band because it is limited by the minimum achievable repetition time (TR). Efforts to improve sensitivity have led to mixed findings (9,11). Therefore, an alternative ncMRI technique for detecting such rapidly varying fields is desirable.

To directly detect the field produced by an alternating current with MRI, Kraus et al. (25) previously proposed

[1]Brain Research Imaging Center, University of Chicago, Chicago, IL 60637.
[2]Center for MRI Research, Academy for Advanced Interdisciplinary Studies, Peking University, Beijing, China.
[3]Beijing City Key Lab for Medical Physics and Engineering, Institute of Heavy Ion Physics, School of Physics, Peking University, Beijing, China.
[4]Wuhan Institute of Physics and Mathematics, Chinese Academy of Sciences, Wuhan, China.
[5]GE Healthcare MR Research China, Beijing, China.
[6]McGovern Institute for Brain Research, Peking University, Beijing, China

Grant sponsor: China's National Strategic Basic Research Program; Grant number: 973 2012CB720700; Grant sponsor: Natural Science Foundation of China; Grant numbers: 81227003, 81430037, and 31421003; Grant sponsor: NIH; Grant number: R21EB015023.

*Correspondence to: Jia-Hong Gao, Ph.D., Center for MRI Research, Peking University, Beijing, China 100871. E-mail: jgao@pku.edu.cn.

Received 9 July 2014; revised 14 October 2014; accepted 7 November 2014
DOI 10.1002/mrm.25553
Published online 8 March 2015 in Wiley Online Library (wileyonlinelibrary.com).

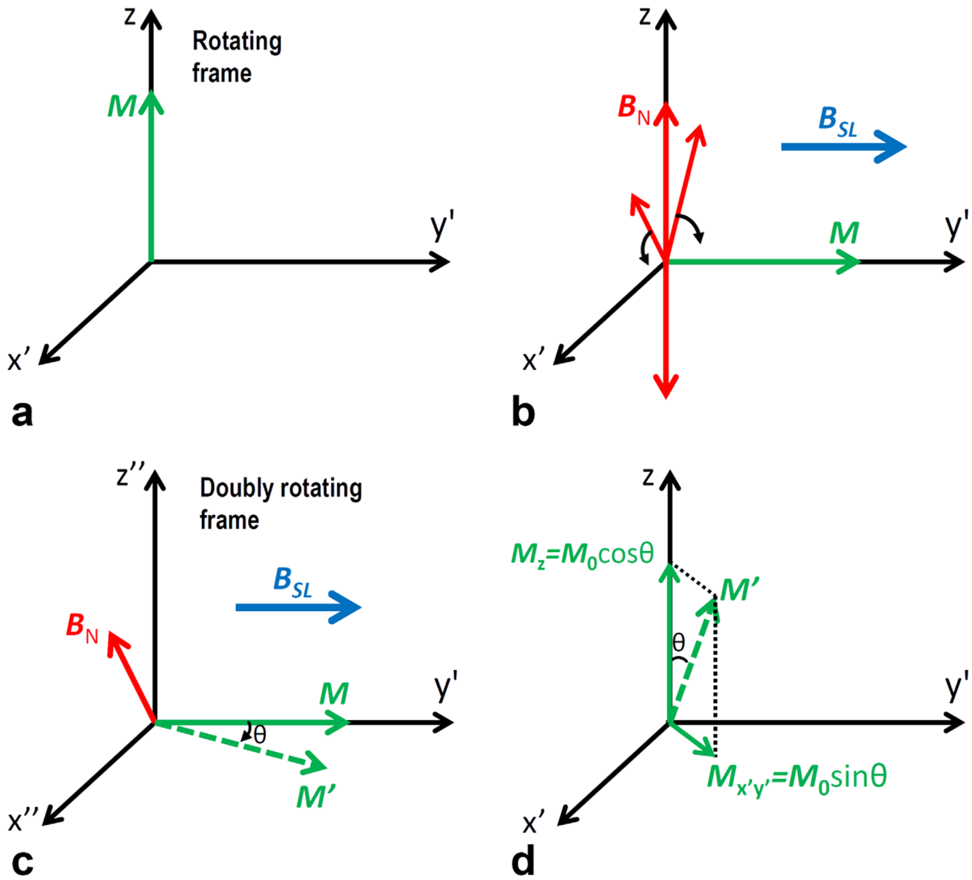

FIG. 1. Evolution of the net magnetization under the influence of an oscillating field B_N during the SIRS pulse sequence. (a) In the rotating frame x'y'z, the net magnetization M initially lies along the direction of $\boldsymbol{B}_0$. (b) M is then flipped into the y' direction with a 90-degree pulse, and a continuous spin-lock pulse $\boldsymbol{B}_{SL}$ is applied in the same direction to prevent spin dispersion. The magnitude of $\boldsymbol{B}_{SL}$ is matched with the frequency of the oscillatory neural field of interest $\boldsymbol{B}_N$. $\boldsymbol{B}_N$ can be decomposed into two rotating vectors with the same frequency and opposite directions. (c) It is now more convenient to visualize the spin evolution in a doubly rotating frame (denoted as x"y'z"), which rotates simultaneously at a frequency of $\frac{B_0}{\gamma}$ around z and at a frequency of $\frac{B_{SL}}{\gamma}$ around y'. In this frame, one of the components of $\boldsymbol{B}_N$ appears stationary and serves to rotate M away from the spin-lock direction y' by a small angle. (d) At the end of $\boldsymbol{B}_{SL}$, M is flipped back to the longitudinal direction, and the reduction in $\boldsymbol{M}_z$ provides the signal contrast.

a different approach employing an ultralow field combined with a superconducting quantum interference device (SQUID) (26) and demonstrated successful in-phantom experiments. In their acquisition scheme, the sample was prepolarized with a separate field (~ 40 mT) before it was placed in an ultralow field (~ 97 μT) and an oscillatory field. The latter field was used to mimic the oscillatory neural field and was positioned orthogonal to the ultralow field. When the Larmor frequency of the ultralow field matches the frequency of the neural field, a resonance condition occurs that serves to tilt the initial magnetization. Although this method offers several advantages, it requires the use of a SQUID detector and a prepolarizing device. It also suffers from the low-detection sensitivity intrinsic to low-field imaging.

Based on Kraus et al.'s approach (25), Witzel et al. cleverly employed a long spin-lock pulse to effectively lower the Larmor frequency in the doubly rotating frame to below 100 Hz on a commercial MRI scanner and demonstrated its effectiveness in phantom studies (27). The authors named this approach the stimulus-induced rotary saturation (SIRS) mechanism. Halpern-Manners et al. later improved on this method by incorporating ramped and phase-modulated spin-lock pulses (28). In the SIRS method (illustrated in Figure 1; see figure caption for more details), the net magnetization M (Fig. 1a) is first flipped into the transverse plane, and a spin-lock pulse $\boldsymbol{B}_{SL}$ is applied in the same direction as M for a duration of T_{SL} (Fig. 1b). The magnitude of $\boldsymbol{B}_{SL}$ is carefully tuned so that its Larmor frequency matches the frequency of the oscillatory neural field of interest. Consequently, a resonance condition occurs and M is coherently rotated away from the spin-lock direction by a small angle, giving rise to the signal contrast (Fig. 1c). At the end of the spin-lock pulse, M is flipped back to the longitudinal direction, and the reduction in the longitudinal magnetization $\boldsymbol{M}_z$ provides the signal contrast for subsequent imaging (Fig. 1d).

In the present study, we seek to improve the sensitivity of the SIRS mechanism by using a modified sequence involving an oscillatory stimulus $\boldsymbol{B}_N$. The stimulus-induced rotation causes M to deviate from its equilibrium direction by an angle of $\theta = \frac{\gamma B_N T_{SL}}{2}$, where γ is the gyromagnetic ratio and B_N is the amplitude of the

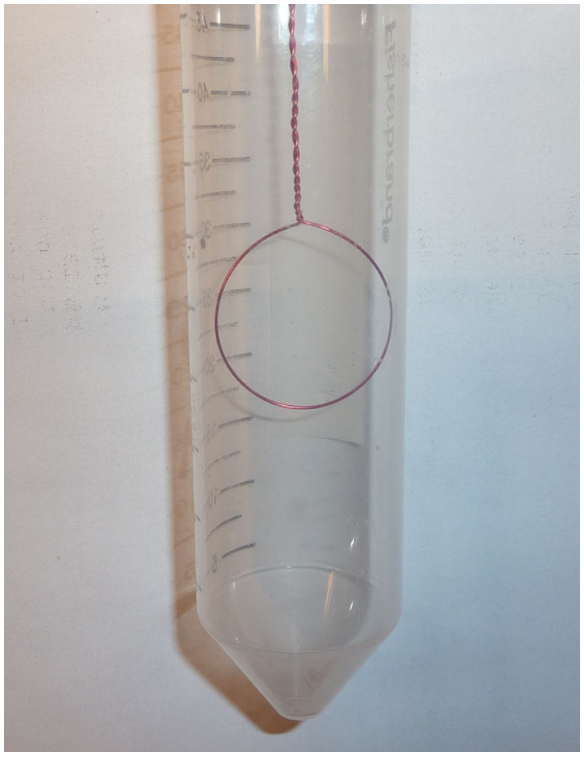

FIG. 2. The neuronal current MRI phantom used in this study consisted of a single-loop, circular copper coil, 2.5 cm in diameter, inserted into a plastic tube filled with 3.0 mM $NiCl_2$ solution.

oscillatory neural field. In the original SIRS approach, the reduction in $\boldsymbol{M}_z$ is used as contrast, which is proportional to $1 - \cos\theta \approx \frac{\theta^2}{2}$. The buildup of magnetization in the transverse plane, $\boldsymbol{M}_{xy}$, is removed with a crusher gradient pulse. However, the magnitude of $\boldsymbol{M}_{xy}$ is proportional to $\sin\theta \approx \theta$, which is much larger than $\frac{\theta^2}{2}$, given that θ is usually a very small angle. For example, assuming an oscillatory field B_N of 1 nT, and $T_{SL} = 200$ ms, using θ instead of $\frac{\theta^2}{2}$ represents a 37-fold increase in the contrast. Therefore, we propose to use $\boldsymbol{M}_{xy}$ instead of $\boldsymbol{M}_z$ as the signal source for the subsequent imaging. This is realized by placing an EPI readout immediately after the preparation pulses, which included a $90°_{+x}$ pulse, a long spin-lock pulse $\boldsymbol{B}_{SL,+y}$, and a $90°_{-x}$ pulse. No excitation pulse is needed because the transverse magnetization is created by the SIRS effect. In this regard, the present approach is similar to the previous, ultralow field approach (25).

METHODS

Phantom

A single loop coil with a 2.5-cm diameter (Fig. 2) was used to produce an oscillating magnetic field. The coil was made of 26-gauge copper wire coated with an insulation layer. The field strength that is reported in the Results section was calculated at the center of the coil. Oscillatory currents were produced using a high-speed function generator (EW-26864-20, Cole-Parmer, Vernon Hills, IL). The coil was placed at the center of a plastic tube filled with 3.0-mM $NiCl_2$ solution. The T_1 and T_2 constants of the phantom were measured to be ~ 450 ms and ~ 325 ms, respectively. The phantom was positioned in the scanner such that the plane of the coil was perpendicular to $\boldsymbol{B}_0$. Therefore, the magnetic field in the plane of the coil was parallel with $\boldsymbol{B}_0$. The longitudinal and transverse relaxation time in the rotating frame $T_{1\rho}$ and $T_{2\rho}$ were measured using methods described previously (29,30).

ncMRI Acquisition

The ncMRI scans were performed on a 3-Tesla (3T) Philips Achieva scanner (Philips Healthcare, The Netherlands) with an eight-channel sensitivity-encoding head coil. The modified SIRS sequence with the simple spin-lock scheme ($90°_{+x}$–$B_{SL,+y}$–$90°_{-x}$) was found to produce severe image artifacts due to the field inhomogeneity ($\Delta\boldsymbol{B}_0$) in the main magnetic field; hence, a modified $\Delta\boldsymbol{B}_0$-insensitive sequence (28,31) was used for imaging, which consisted of five preparation pulses ($90°_{+x}$–$B_{SL,+y}$–$180°_{+y}$–$B_{SL,-y}$–$90°_{-x}$). The acquisition sequence is illustrated in Figure 3. The preparation pulses served to encode the external oscillatory field and were followed by a gradient echo–echo planar imaging readout. A 180-degree RF pulse sandwiched by two equal gradients could be used to achieve slice selection (32). However, for the actual experiments in this study, no slice selection was performed, and two saturation bands were used to define the slice position and thickness immediately before the spin-lock pulses. The following acquisition parameters were used: $T_{SL} = 200$ ms, TR = 415 ms, echo time (TE) = 48 ms, field of view (FOV) 0 = 96 × 96 mm^2, in-plane resolution = 1.2 × 1.2 mm^2, slice thickness = 6 mm, and slice number = 1. Second-order volume shimming was performed to reduce B_0 inhomogeneity. For the detection of currents, 800 images were acquired with 10 dummy scans, resulting in a total scan time of 5.6 min. A block experimental design was used in which the oscillatory field was turned on or off every 100 TR with eight blocks.

Data Analysis

The ncMRI data was analyzed in a voxel-wise manner. The time series at each voxel was first high-pass filtered

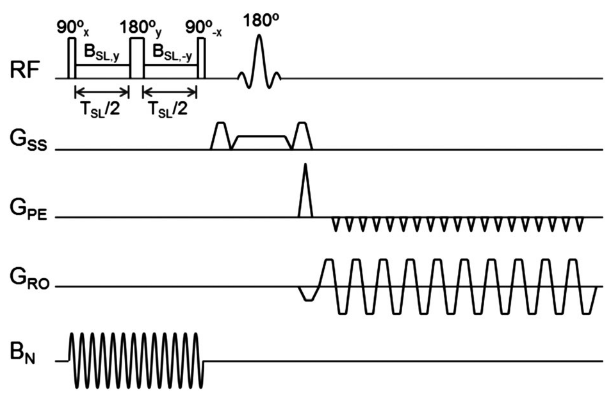

FIG. 3. The modified SIRS sequence. Compared to the previous SIRS approaches, no excitation pulse is used in this sequence, and a 180° pulse sandwiched between two equal gradients was used for slice selection. RF, radio frequency; SIRS, stimulus induced rotary saturation.

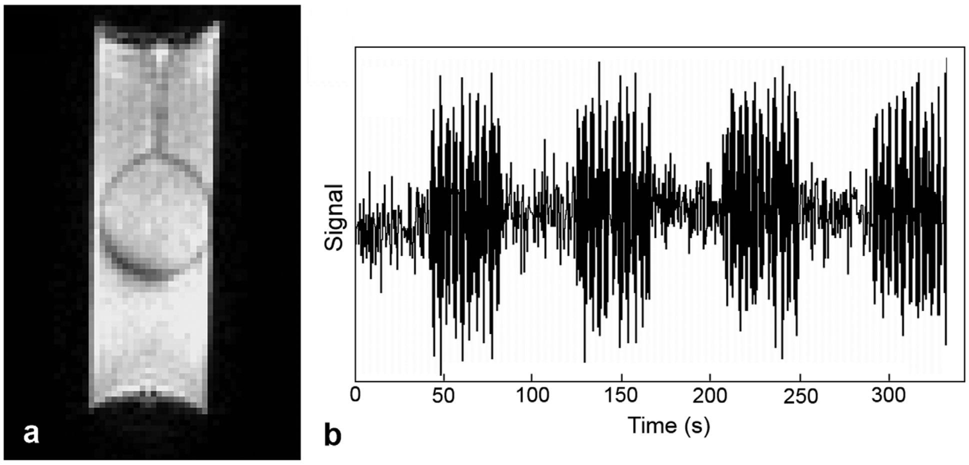

FIG. 4. ncMRI phantom image and time course. (a) A representative ncMRI phantom image acquired with a $\Delta \boldsymbol{B}_0$-insensitive spin-lock pulse sequence (90°_{+x} $-B_{SL,+y}-180^{\circ}_{+y}-B_{SL,-y}-90^{\circ}_{-x}$) and no excitation pulse. (b) The time course of the ncMRI signal from a single voxel at the center of the coil in a. A 3-nT oscillatory field was turned on and off for even and odd number of blocks respectively. ncMRI, neuronal current MRI.

at 0.1 Hz to remove any slow temporal drift. A student *t* test was then performed to compare the on-blocks to the off-blocks to identify the active voxels. As shown in the Results section, the effect of the external oscillatory field is not a change in the signal magnitude of the MR time course, as is the case for previous SIRS method, but instead is an increased fluctuation in the time course. Therefore, the temporal standard deviation (SD) was calculated for the time course in each block, and a two-sample *t* test was used to compare the SDs between the on- and off-blocks.

Alternatively, because the applied external field had an exact sinusoidal form, its phase information may be exploited to increase the statistical power. For example, with a 100-Hz external field and TR = 415 ms, any two adjacent data points in the ncMRI time series would have opposite phases, and the effective magnetic fields in the doubly rotating frame (B_N in Fig. 1c) would point in opposite directions. Hence, the oscillatory field would have opposite effects on the baseline signal level; that is, the MR signal magnitude would be increased in one image and decreased in the next one. To use this knowledge, difference in signal magnitude was calculated between adjacent time points. Then, a two-sample *t* test was used to compare the obtained signal difference between the on- and off-blocks. This approach was found to produce slightly higher statistical significance than the first approach. However, it may not be as useful for in vivo studies due to the lack of phase coherence in real neural oscillations.

RESULTS

ncMRI Images and Time Course

A ncMRI image of a phantom that consists of a cylindrical tube containing a copper wire loop acquired using this sequence is shown in Figure 4a. The experiment was performed with a spin-lock field of which the Larmor frequency was 100 Hz and the duration was 200 ms. It should be noted that the signal magnitude is nonzero in the phantom, although no excitation pulse or oscillatory field was applied. This nonzero signal was partially caused by T_1 recovery during the spin-lock time. In addition, the inhomogeneity of the $\boldsymbol{B}_0$ and $\boldsymbol{B}_1$ fields may also lead to a residual transverse magnetization. This signal was used as the baseline signal in the ncMRI time course and allowed the structure of the phantom to be visible in Figure 4a. It should be noted that this signal level is very low compared to the signal level in the original SIRS approach, in which a 90-degree excitation pulse was used after the spin-lock pulse to form images.

Figure 4b shows the ncMRI signal time course obtained from a block design experiment with eight blocks and 100 time points in each block (see Methods). The time course shown here corresponds to the signal from a single voxel at the center of the copper coil seen in Figure 4a. An oscillatory field of 3 nT and 100 Hz was turned on every other block. It can be seen that the external field did not cause an elevated signal level; instead, it appeared to cause an increase in the fluctuation in the time course. This is because there are two sources contributing to the signal during the on-blocks: 1) the baseline signal due to the inhomogeneity in the $\boldsymbol{B}_0$ and $\boldsymbol{B}_1$ fields, as was discussed above; and 2) the transverse magnetization caused by the oscillating current. Whereas the first signal has a fixed phase, the phase of the second signal varies within each TR; therefore, the relative phase between the two signals is uncertain. As a result, the second signal sometimes enhances the baseline signal when they are in phase and sometimes reduces the baseline signal when they are out of phase. This causes the time course during the on-blocks to have an increased temporal SD compared to the off-blocks. It is also clear from Figure 4b that a 3-nT field can cause large enough contrast for ncMRI detection.

Detection Sensitivity

P-static maps obtained from a 5.6-min acquisition are shown in Figure 5 for field strengths from 0.25 nT to 1.0 nT at 100 Hz. With $B_N = 1.0$ nT (Fig. 5a) and $B_N = 0.5$ nT (Fig. 5b), strong activation could be seen at the center of the coil at $P < 0.001$ (uncorrected) level. For $B_N = 0.25$ nT (Fig. 5c), the activation was less statistically significant. But with a relaxed threshold of $P < 0.03$ (uncorrected), activation could still be reliably detected at the center of the coil, with a few false positive voxels found outside

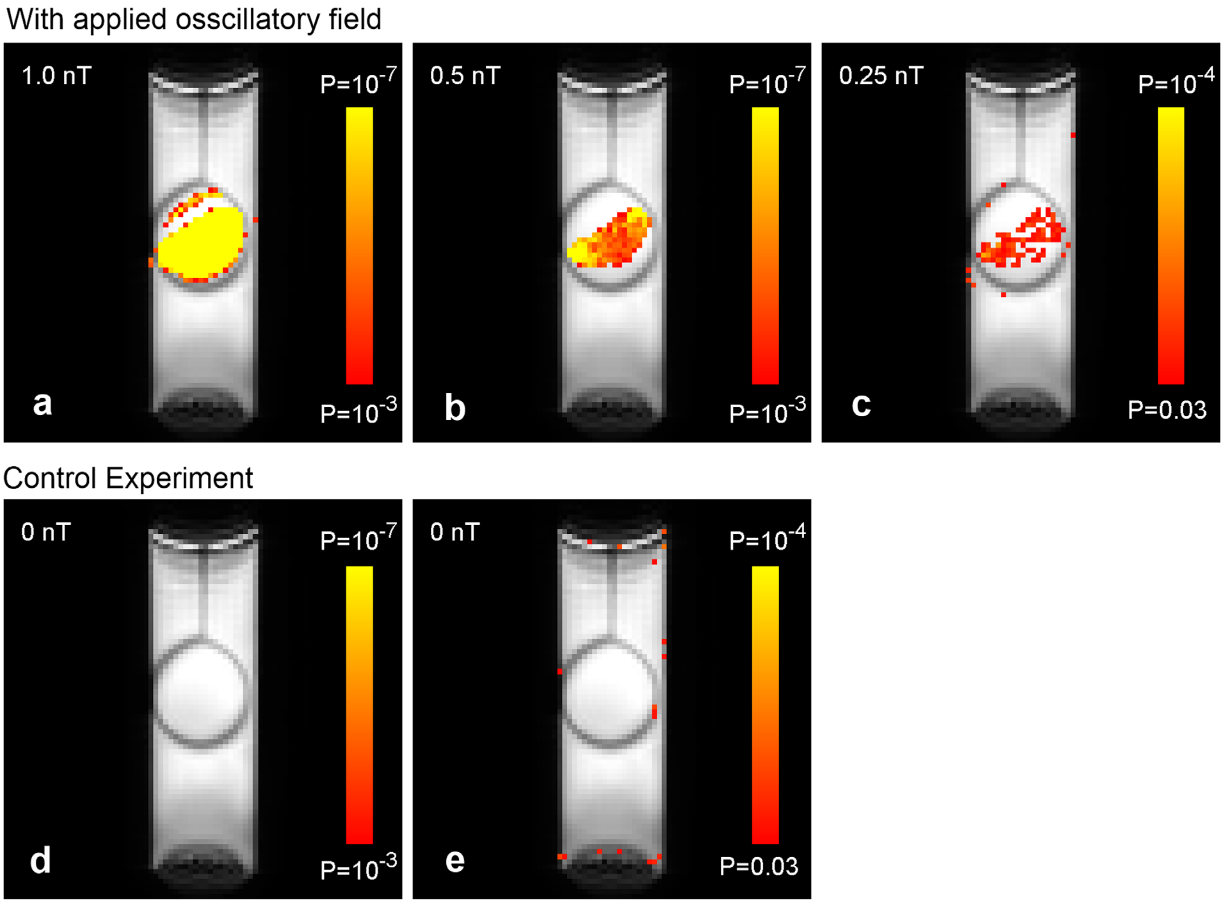

FIG. 5. ncMRI-detection sensitivity. P-static maps (uncorrected, shown in color) are overlaid on ncMRI images. Results are shown for an applied external oscillatory field at 100 Hz with magnitude of 1.0 nT (a), 0.5 nT (b), and 0.25 nT (c). The threshold for the statistic map is $P < 0.001$ in panels a and b, and $P < 0.03$ in panel c. Results of a control experiment with no external field applied are also shown with the threshold at $P < 0.001$ (d) and $P < 0.03$ (e). ncMRI, neuronal current MRI; nT, nanotesla

of the coil. For comparison, a control experiment with no external field applied found no false positive voxels at the $P < 0.001$ level (Fig. 5d) and a few scattered false positive voxels at the $P < 0.03$ level (Fig. 5e).

Frequency Response

It is useful to know the frequency response of the ncMRI pulse sequence for in vivo applications for which the target signal spans over a frequency range. In this experiment, the frequency of the spin-lock pulse was fixed at 100 Hz, whereas the frequency of the external field was varied from 75 Hz to 125 Hz. Two hundred time points were acquired for each frequency, with identical parameters as the previous experiments, and a field strength of 6.0 nT was used. The temporal SD of the time course was calculated for each frequency, and the result is shown in Figure 6. As expected, a peak center around 100 Hz was observed. The full width at half maximum was found to be 4 to 6 Hz, which is reasonable for measuring neural oscillation at 100 Hz. In some cases, a secondary peak was also observed between 90 Hz to 95 Hz. The origin of such a peak is not entirely clear yet. One possible explanation is the Bloch–Siegert shift (33), where the counter-rotating component of the linearly polarizing field causes a slight shift in the effective resonance frequency. However, such a shift is likely to be too small to explain the observed frequency difference (a few Hz). A more likely explanation is that the presence of the copper coil causes inhomogeneity in the B_1 field; therefore, it is possible that the magnitude of the spin-lock pulse deviates from its intended value at some locations within the coil, leading to an altered resonance frequency.

Linearity

One difference between the modified SIRS sequence and the original SIRS sequence is that the signal contrast would be a linear function of the oscillating field in the present approach, whereas the contrast would be a quadratic function of the oscillating field in the original SIRS method. To test the linearity relationship, we measured the contrast to noise ratio (CNR) of the ncMRI time courses with external field $B_N = 1$ nT, 2 nT, 4 nT, and 8 nT, both at 100 Hz and 25 Hz. The CNR was calculated as the ratio of the mean temporal SD of the on-blocks to that of the off-blocks, and the results are shown in Figure 7. An approximately linear relationship was observed between the CNR and B_N at both frequencies, confirming the hypothesis as posed. The calculated CNR did not go to zero at $B_N = 0$ because the thermal noise

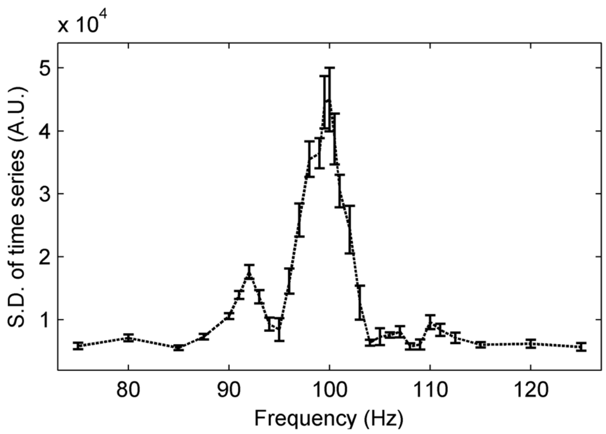

FIG. 6. Frequency response of the modified SIRS sequence. The frequency of the spin-lock pulse was fixed at 100 Hz, while the frequency of the external field was varied from 75 Hz to 125 Hz. The temporal SD of the time course (in arbitrary unit) was plotted as a function of the frequency of the applied field. SD, standard deviation; SIRS, stimulus induced rotary saturation.

also contributes to the calculation of contrast in our definition of the CNR. The contrast was slightly lower at 25 Hz than at 100 Hz because the spin-lock field is lower at 25 Hz and therefore less efficient in locking the magnetization. But sufficient CNR was still achieved at 25 Hz, indicating the feasibility of extending the present approach into low frequency ranges. The relaxation of M in the doubly rotating frame in the spin-lock direction (y′ in Fig. 1c) can be described by $\exp\left(-\frac{T_{SL}}{T_{1\rho}}\right)$. $T_{1\rho}$ is known to increase with the magnitude of $\boldsymbol{B}_{SL}$. $T_{1\rho}$ approaches T_2 as $\boldsymbol{B}_{SL}$ approaches zero and increases to a maximum of T_1 as $\boldsymbol{B}_{SL}$ increases (29,30). Therefore, the signal contrast is lowered with a lower resonance frequency. The relaxation of M in the doubly rotating frame in the transverse plane (x″z″ in Fig. 1c) can be described by $\exp\left(-\frac{T_{SL}}{T_{2\rho}}\right)$. Unlike $T_{1\rho}$, $T_{2\rho}$ is known to be only weakly affected by the magnitude of $\boldsymbol{B}_{SL}$ (30). However, because the magnetization in the transverse plane is gradually built up during T_{SL} instead of at the beginning of T_{SL}, the spin dispersion due to inhomogeneity in $\boldsymbol{B}_{SL}$ will not be completely refocused at the end of T_{SL}. The amount of spin dispersion, and hence signal loss, increases with the inhomogeneity in $\boldsymbol{B}_{SL}$, which is likely to increase with $\boldsymbol{B}_{SL}$. Therefore, it is likely that variation in $\boldsymbol{B}_{SL}$ would have the opposite effects on the relaxations in the longitudinal and transverse directions. Our results suggest that the former effect is more important.

DISCUSSION

In this study, we have demonstrated that an external oscillatory field could be used as an excitation pulse under a spin-locked condition to encode the MR signal. With a 5.6-min scan, magnetic fields as low as 0.25 nT could be reliably detected. Such detection sensitivity is better than that achieved with the original SIRS approach (27,28). Most importantly, it should be noted that our experiment was conducted with conditions closer to those of in vivo imaging. In Witzel et al.'s study, a field of 1.0 nT was detected with a 7-min experiment (27). The phantom used in that study had a $T_{1\rho}$ value of 980 ms, which helped minimize magnetization relaxation in the doubly rotating frame. The $T_{1\rho}$ of our phantom (300–305 ms) was closer to that of human gray matter (~99±1 ms (29)). In Halpern-Manners et al.'s study, activation was detected for a coil producing 0.46 nT field at its center, with 8- to 12-min experiments (28). However, in their results, most of the activated voxels appeared to be located adjacent to the current-carrying coil for which the field would be much higher than that at the center of the coil. In addition, their experiments were performed on 7T spectrometers using coils with higher sensitivity. In contrast, our experiment was performed with a 3T whole-body scanner and a head receiver coil, and activation was reliably detected at the center of the current-carrying coil at 0.25 nT level. A direct comparison of the detection sensitivity between the modified and the original SIRS sequences is provided in Appendix 1. (online only).

The pulse sequence proposed in the present study has several advantages compared with the previous SIRS approaches. Firstly, higher contrast could be achieved because of the θ versus $\frac{\theta^2}{2}$ effect, as discussed previously. Secondly, the proposed sequence would help lower physiological noise when applied to human studies. In human fMRI studies, the physiological noise dominates over the thermal noise and is proportional to the signal magnitude (34). In the modified SIRS sequence, because the MR signal is contributed by the weak oscillatory field and no additional excitation pulse was applied, the absolute signal level is very low compared to those of the conventional MRI studies. The proposed pulse sequence will greatly reduce the physiological noise in human studies. Thirdly, the proposed sequence allows for faster image acquisition with short TR. At the end of the preparation pulses, the net magnetization is returned to the z-direction and its magnitude is only reduced by the

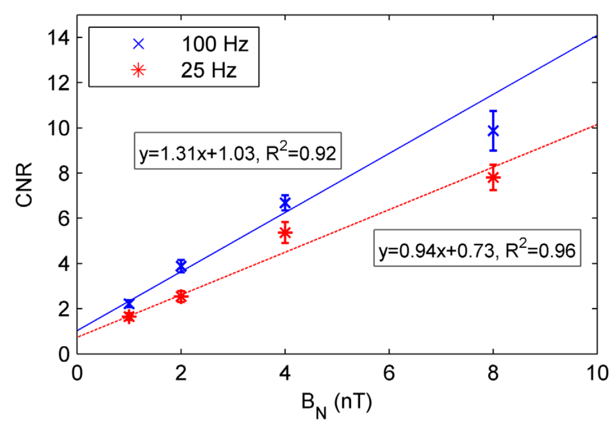

FIG. 7. Contrast of the modified SIRS sequence as a function of the magnitude of the applied field. Data are shown for $B_N = 1$ nT, 2 nT, 4 nT, and 8 nT at frequencies of 100 Hz and 25 Hz. The contrast was calculated as the ratio of the mean temporal standard deviation of the on-blocks to that of the off-blocks. The straight lines are the least-square linear fit with the error bar sizes taken into consideration. CNR = contrast to noise ratio; SIRS, stimulus induced rotary saturation.

amount of $T_{1\rho}$ relaxation during T_{SL}; therefore, sufficient $\boldsymbol{M}_z$ remains for acquiring the next image. In contrast, the original SIRS sequence uses 90-degree excitation pulses after the preparation pulses to produce maximum contrast, and this approach eliminates $\boldsymbol{M}_z$. Thus, its TR is limited by the T_1 recovery. However, after the preparation pulses, the original SIRS sequence preserves the signal contrast in the longitudinal direction, which features a slower decay and is potentially beneficial for multislice acquisition. Lastly, the proposed sequence is insensitive to the BOLD effect, which was a major confounding variation in most previous ncMRI human studies. In the statistical analysis presented, only the SD of the MR time course or the signal difference between two adjacent images is used and not the absolute signal level. Thus, a slow drift in the baseline signal level has a minimum impact on the result. However, the current approach is susceptible to spin dephasing during T_{SL}, where inhomogeneity in the $\boldsymbol{B}_1$ field would lead to different precession rate of M at different locations in the rotating frame. This is likely the reason why the sensitivity of our experiments, although significantly improved, was still not as high as the theoretical prediction of the θ versus $\frac{\theta^2}{2}$ effect.

A $\Delta\boldsymbol{B}_0$-insensitive preparation sequence consisting of five RF pulses (Fig. 3) was used in our experiments. It was previously used to reduce image artifacts related to $\boldsymbol{B}_0$ inhomogeneity. In the present study, it also served to refocus the transverse magnetization in the doubly rotating frame ($\boldsymbol{M}_{x''z''}$ in Fig. 1c) during T_{SL}. However, it should be pointed out that this approach also reduces the signal contrast compared to original SIRS approach with three radio frequency (RF) pulses (26), in which the magnetization in the doubly rotating frame is flipped by $\boldsymbol{B}_N$ by an angle of $\theta = \gamma B_N T_{SL/2}$. With the $\Delta\boldsymbol{B}_0$-insensitive sequence, the situation is more complicated because the direction of $\boldsymbol{B}_{SL}$ is inverted at $\frac{T_{SL}}{2}$. Assuming that the phase of $\boldsymbol{B}_N$ (the angle between $\boldsymbol{B}_N$ and z'' in Fig. 1) is φ and that $\frac{T_{SL}}{2}$ is an integral number of times the period of the spin-lock pulse, which was the case in our experiment, then after $\boldsymbol{B}_{SL}$ is inverted, the new $\boldsymbol{B}_N$ will have a phase of $-\varphi$. Ignoring any inaccuracy in $\boldsymbol{B}_0$ and $\boldsymbol{B}_1$, the magnetization at the end of T_{SL} can be written as

$$\boldsymbol{M}(T_{SL}) = R_{-\varphi}(\theta/2)R_{\varphi}(-\theta/2)\boldsymbol{M}(0), \quad [1]$$

where R_φ and $R_{-\varphi}$ are the rotation matrices around $\boldsymbol{B}_N$ during first and second halves of T_{SL}, $\frac{\theta}{2}$ is the angle by which $\boldsymbol{M}$ is rotated during $\frac{T_{SL}}{2}$, and $\boldsymbol{M}(0) = [0\ M_0\ 0]'$ is the initial magnetization vector. Eq. 1 can be calculated by transformation to the tilted rotating frame:

$$\boldsymbol{M}(T_{SL}) = R_y(-\varphi)R_z(\theta/2)R_y(\varphi)R_y(\varphi)R_z(-\theta/2)R_y(-\varphi)\boldsymbol{M}(0), \quad [2]$$

in which $R_y(\varphi)$ and $R_z(\varphi)$ are the rotation matrices around the y and z direction. After simplification, it can be shown that the transverse magnetization at the end of T_{SL} is

$$M_{xz}(T_{SL}) = \sqrt{2}\cos\varphi\sin(\theta/2)M_0. \quad [3]$$

Thus, M_{xz} is reduced by a factor of $\frac{|\cos\varphi|}{\sqrt{2}}$ with the $\Delta\boldsymbol{B}_0$-insensitive sequence. Because the phase φ is a random number that changes for every TR, the mean ratio is $\frac{\sqrt{2}}{\pi} \cong 0.45$. Therefore, the $\Delta\boldsymbol{B}_0$-insensitive sequence reduces the signal contrast by more than half. But the associated image artifacts and baseline signal-level reduction make it beneficial to the overall detection sensitivity.

CONCLUSION

Given the sensitivity of the modified SIRS sequence achieved in our phantom, it might be feasible to attempt the detection of neural oscillations in humans with this technique. An equivalent current, dipole moments larger than 100 nAm, has been recorded for the alpha activity with magneto encephalographic (MEG) (35). This corresponds to a magnetic field of 2.5 nT at a distance of 2 mm from the dipole source. If the source is more extended than a few millimeters, the actual field will be lower than this number; however, the MEG measurement on the scalp suffers from cancellation effect and tends to underestimate local fields. The exact field strength depends on the geometry of local neuronal trees and is not straightforward to estimate. Of course, the $\boldsymbol{B}_0$ and $\boldsymbol{B}_1$ inhomogeneity-related artifacts will be more severe in the in vivo brain than in our phantom, so it is likely that the actual effective magnitude approximates what is necessary for successful detection.

REFERENCES

1. Jasanoff A. Bloodless FMRI. Trends Neurosci 2007;30:603–610.
2. Singh M. Sensitivity of MR phase shift to detect evoked neuromagnetic fields inside the head. IEEE Trans Nucl Sci 1994;41:349–351.
3. Bodurka J, Bandettini PA. Toward direct mapping of neuronal activity: MRI detection of ultraweak, transient magnetic field changes. Magn Reson Med 2002;47:1052–1058.
4. Konn D, Gowland P, Bowtell R. MRI detection of weak magnetic fields due to an extended current dipole in a conducting sphere: a model for direct detection of neuronal currents in the brain. Magn Reson Med 2003;50:40–49.
5. Pell GS, Abbott DF, Fleming SW, Prichard JW, Jackson GD. Further steps toward direct magnetic resonance (MR) imaging detection of neural action currents: optimization of MR sensitivity to transient and weak currents in a conductor. Magn Reson Med 2006;55:1038–1046.
6. Xiong J, Fox PT, Gao J-H. Directly mapping magnetic field effects of neuronal activity by magnetic resonance imaging. Hum Brain Mapp 2003;20:41–49.
7. Bianciardi M, Di Russo F, Aprile T, Maraviglia B, Hagberg GE. Combination of BOLD-fMRI and VEP recordings for spin-echo MRI detection of primary magnetic effects caused by neuronal currents. Magn Reson Imaging 2004;22:1429–1440.
8. Chu R, de Zwart JA, van Gelderen P, Fukunaga M, Kellman P, Holroyd T, Duyn JH. Hunting for neuronal currents: absence of rapid MRI signal changes during visual-evoked response. Neuroimage 2004;23:1059–1067.
9. Konn D, Leach S, Gowland P, Bowtell R. Initial attempts at directly detecting alpha wave activity in the brain using MRI. Magn Reson Imaging 2004;22:1413–1427.
10. Liston AD, Salek-Haddadi A, Kiebel SJ, Hamandi K, Turner R, Lemieux L. The MR detection of neuronal depolarization during 3-Hz spike-and-wave complexes in generalized epilepsy. Magn Reson Imaging 2004;22:1441–1444.
11. Mandelkow H, Halder P, Brandeis D, Soellinger M, de Zanche N, Luechinger R, Boesiger P. Heart beats brain: the problem of detecting alpha waves by neuronal current imaging in joint EEG–MRI experiments. Neuroimage 2007;37:149–163.
12. Parkes LM, de Lange FP, Fries P, Toni I, Norris DG. Inability to directly detect magnetic field changes associated with neuronal activity. Magn Reson Med 2007;57:411–416.

13. Chow LS, Dagens A, Fu Y, Cook GG, Paley MNJ. Comparison of BOLD and direct-MR neuronal detection (DND) in the human visual cortex at 3T. Magn Reson Med 2008;60:1147–1154.
14. Tang L, Avison MJ, Gatenby JC, Gore JC. Failure to direct detect magnetic field dephasing corresponding to ERP generation. Magn Reson Imaging 2008;26:484–489.
15. Sundaram P, Wells WM, Mulkern RV, Bubrick EJ, Bromfield EB, Münch M, Orbach DB. Fast human brain magnetic resonance responses associated with epileptiform spikes. Magn Reson. Med 2010;64:1728–1738.
16. Bandettini P, Petridou N, Bodurka J. Direct detection of neuronal activity with MRI: fantasy, possibility, or reality? Appl Magn Reson 2005;29:65–88.
17. Luo Q, Lu H, Lu H, Senseman D, Worsley K, Yang Y, Gao JH. Physiologically evoked neuronal current MRI in a bloodless turtle brain: detectable or not? Neuroimage 2009;47:1268–1276.
18. Hamalainen M, Hari R, Ilmoniemi R, Knuutila J, Lounasmaa O. Magnetoencephalography theory, instrumentation, and applications to non-invasive studies of the working human brain. Rev Mod Phys 1993;65:413–497.
19. Gray CM, König P, Engel AK, Singer W. Oscillatory responses in cat visual cortex exhibit inter-columnar synchronization which reflects global stimulus properties. Nature 1989;338:334–337.
20. Pfurtscheller G, Lopes da Silva FH. Event-related EEG/MEG synchronization and desynchronization: basic principles. Clin Neurophysiol 1999;110:1842–1857.
21. Murthy VN, Fetz EE. Oscillatory activity in sensorimotor cortex of awake monkeys: synchronization of local field potentials and relation to behavior. J Neurophysiol 1996;76:3949–3967.
22. Klimesch W. EEG alpha and theta oscillations reflect cognitive and memory performance: a review and analysis. Brain Res Brain Res Rev 1999;29:169–195.
23. Lee K-H, Williams LM, Breakspear M, Gordon E. Synchronous gamma activity: a review and contribution to an integrative neuroscience model of schizophrenia. Brain Res Brain Res Rev 2003;41:57–78.
24. Canolty RT, Edwards E, Dalal SS, Soltani M, Nagarajan SS, Kirsch HE, Berger MS, Barbaro NM, Knight RT. High gamma power is phase-locked to theta oscillations in human neocortex. Science 2006; 313:1626–1628.
25. Kraus Jr R, Volegov P, Matlachov A, Espy M. Toward direct neural current imaging by resonant mechanisms at ultra-low field. Neuroimage 2008;39:310–317.
26. Volegov P, Matlachov AN, Espy MA, George JS, Kraus RH. Simultaneous magnetoencephalography and SQUID detected nuclear MR in microtesla magnetic fields. Magn Reson Imaging 2004;52:467–470.
27. Witzel T, Lin F-H, Rosen BR, Wald LL. Stimulus-induced rotary saturation (SIRS): a potential method for the detection of neuronal currents with MRI. Neuroimage 2008;42:1357–1365.
28. Halpern-Manners NW, Bajaj VS, Teisseyre TZ, Pines A. Magnetic resonance imaging of oscillating electrical currents. Proc Natl Acad Sci U S A 2010;107:8519–8524.
29. Borthakur A, Wheaton AJ, Gougoutas AJ, Akella SVS, Regatte RR, Charagundla SR, Reddy R. In vivo measurement of T1rho dispersion in the human brain at 1.5 tesla. J Magn Reson Imaging 2004;19:403–409.
30. Wheaton AJ, Borthakur A, Corbo MT, Moonis G, Melhem E, Reddy R. T2rho-weighted contrast in MR images of the human brain. Magn Reson Med 2004;52:1223–1227.
31. Witschey WRT, Borthakur A, Elliott MA, Mellon E, Niyogi S, Wallman DJ, Wang C, Reddy R. Artifacts in T1ρ-weighted imaging: compensation for B1 and B0 field imperfections. J Magn Reson 2007; 186:75–85.
32. Scott GC, Joy ML, Armstrong RL, Henkelman RM. RF current density imaging in homogeneous media. Magn Reson Med 1992;28:186–201.
33. Bloch F, Siegert A. Magnetic resonance for nonrotating fields. Phys Rev 1940;57:522–527.
34. Krüger G, Glover GH. Physiological noise in oxygenation-sensitive magnetic resonance imaging. Magn Reson Med 2001;46:631–637.
35. Ciulla C, Takeda T, Endo H. MEG characterization of spontaneous alpha rhythm in the human brain. Brain Topogr 1999;11:211–222.

SUPPORTING INFORMATION

Additional Supporting Information may be found in the online version of this article.

Appendix S1. Detection of Sub-Nanotesla Oscillatory Magnetic Fields Using MRI.

Figure S1. The neuronal current MRI phantom used in the comparison study. A circular copper coil was wound around a plastic tube in a plane perpendicular to the long axis of the tube.

Figure S2. Statistical results of the modified and original SIRS sequence. P-static maps (uncorrected, shown in color) are overlaid on a structural image with the same voxel size. Results are shown for an applied external oscillatory field at 100 Hz with magnitudes of 1.0 nT (a and c), and 2.0 nT (b and d) in the center of the loop. The detection thresholds were set at $P < 0.001$ for the modified SIRS method (a and b) and $P < 0.01$ for the original SIRS method (c and d). nT, nanotesla; SIRS, stimulus induced rotary saturation.